RSC Advances

PAPER

View Article Online
View Journal | View Issue

Cite this: *RSC Adv.*, 2025, **15**, 19489

Controlled deposition of Pt nanoparticle size modified TiO_2 nanotubes arrays for enhanced indoor air treatment

Khaoula Missaoui,[a] Mohamed Aziz Hajjaji,[ab] Amine Aymen Assadi*[c] and Anouar Hajjaji[a]

Received 2nd March 2025
Accepted 27th May 2025

DOI: 10.1039/d5ra01492a

rsc.li/rsc-advances

Air pollution remains a significant global health challenge, with contaminants like volatile organic compounds (VOCs) and pathogenic bacteria serving as a major contributor. Titanium dioxide nanotubes (TiO_2-NTs) have emerged as promising materials for air purification, owing to their high surface area, photocatalytic activity, and stability. In this context, this study investigates the controlled electrodeposition of platinum (Pt) nanoparticles onto TiO_2-NTs to enhance their photocatalytic properties for indoor air treatment applications. By optimizing the Pt nanoparticle size and distribution, we aim to improve the degradation of VOCs and the inactivation of airborne bacteria. A series of Pt/TiO_2-NTs catalysts with varying Pt nanoparticle sizes were synthesized *via* electrodeposition onto TiO_2-NTs fabricated *via* anodization of titanium foil. The structural and optical properties of the modified nanotubes were characterized using scanning electron microscopy (SEM), transmission electron microscopy (TEM), X-ray photoelectron spectroscopy (XPS), and photoluminescence (PL). The resulting materials exhibited enhanced photocatalytic degradation of VOCs and effective inactivation of *Escherichia coli* (*E. coli*) under visible light irradiation, attributable to the synergistic effects of Pt and TiO_2-NTs. Notably, catalysts decorated with smaller Pt nanoparticles (10–22 nm) demonstrated the highest photocatalytic activity, emphasizing the critical influence of nanoparticle size on performance.

1. Introduction

In recent years, environmental pollution has become one of the most pressing challenges facing humanity on a global scale. Several studies have demonstrated the effectiveness of nanomaterials in water purification, particularly for the removal of bacterial contaminants.[1,2] Building on these advances, the intersection of nanotechnology and environmental science has enabled innovative approaches to address urgent issues in air quality management.[3]

A substantial portion of our daily human activity unfolds within confined environments, primarily in homes and workplaces, where the quality of air is not consistently optimal. This recognition reveals the importance of addressing indoor air quality for the well-being of individuals in these settings. Within enclosed spaces, indoor air quality is compromised by the presence of microorganisms like bacteria and viruses, as well as a diverse array of volatile organic compounds (VOCs). This combination of pollutants poses a significant hazard to both human health and the environment, contributing to the onset of respiratory problems and various other detrimental health effects.

Photocatalytic oxidation presents a promising solution for the efficient removal VOCs during indoor air treatment.[4,5] This process has attracted significant attention due to its efficacy in VOCs) from indoor air, demonstrating its effectiveness even at room temperature and environmental friendliness.[6] Photocatalytic oxidation involves a dynamic interaction between the photocatalyst, light, and pollutants: the photocatalyst must be activated by light irradiation, and pollutants must adsorb onto the surface of the photocatalyst. This dynamic interaction underscores the pivotal role of the photocatalyst in facilitating the degradation of pollutants, offering a viable and sustainable solution for indoor air quality management.[6,7]

Among various nanomaterials, titanium dioxide nanotubes (TiO_2-NTs) are recognized as ideal photocatalysts for both water and air purification,[8,9] owing to their unique nanotubular architecture, high surface area, advanced photocatalytic performance, chemical stability, and low production cost.[10,11] The TiO_2 nanotube structure has attracted considerable interest due to its unique nanotube architecture and large specific surface area.[12,13] These characteristics render it a valuable

[a]*Laboratoire de Photovoltaïque, Centre de Recherches et des Technologies de l'Energie, Technopole de Borj-Cédria, BP 95, Hammam-Lif 2050, Tunisia*

[b]*Ecole Nationale Supérieure de Chimie de Rennes, University of Rennes, CNRS, ISCR—UMR6226, Rennes 35000, France*

[c]*College of Engineering, Imam Mohammad Ibn Saud Islamic University (IMSIU), Riyadh 11432, Saudi Arabia. E-mail: AAAssadi@imamu.edu.sa; Tel: +966 563260210*

material in various functional domains, including applications in solar cells, sensors, and photocatalysts.

The photocatalytic activity of TiO_2-NTs is initiated by the generation of electron–hole pairs; however, rapid recombination of these pairs reduces overall quantum efficiency. Additionally, the relatively wide band gap of TiO_2 (3.2 eV in the anatase phase) restricts its activity to ultraviolet light, which constitutes only 3–5% of sunlight. These limitations hinder the broader application of TiO_2 in environmental remediation. Various strategies have been explored to enhance visible-light responsiveness and to improve charge separation efficiency.[14]

Research indicates that noble metal nanoparticles, including Au, Ag, Pd, Pt,[15] possess the capability to enhance the absorption of visible light by TiO_2 one of the most active metals for photocatalytic enhancement is platinum. It demonstrates the highest work function, leading to the formation of the highest Schottky barrier among the Pt particles. When deposited on TiO_2, Pt serves as an electron trap, facilitating the capture of electrons.[16,17] This process results in a prolonged electron–hole pair separation lifetime. Pt plays an important role in enhancing the separation of photogenerated electron–hole pairs and promoting interfacial charge transfer. Consequently, this improvement in photon utilization efficiency contributes to enhancing the overall photocatalytic performance.

The photocatalytic properties of Pt-modified TiO_2 have been reported to exhibit significant variations depending on factors such as the amount, morphology, and the chemical state of Pt and specially nanoparticle size distribution which strongly influences the catalytic performance of TiO_2.[18] It was reported that small and monodispersed silver nanoparticles (typically 5–10 nm) exhibit the highest photocatalytic and antimicrobial activity.[19] These results show the relationship between nanoparticle properties and their functional performance, implying diverse avenues for optimizing their utility across different applications.

In this work, we present a comprehensive investigation into TiO_2 nanotubes modified by controlled deposition of Pt nanoparticles, evaluating their morphological and optical properties, photocatalytic activity, and antibacterial efficacy. Our results provide valuable insights for the design and optimization of TiO_2-based nanomaterials for enhanced indoor air treatment, as demonstrated by the efficient degradation of ethyl acetate (a model VOC) and the inactivation of *E. coli.* The following sections detail the experimental methods, results, and discussion, offering an in-depth analysis of the performance of Pt-modified TiO_2 nanotubes.

2. Experimental and setup

2.1. Catalyst preparation: fabrication of TiO_2-NTs decorated with Pt nanoparticles

The ordered TiO_2-NTs were fabricated by an electrochemical anodic oxidation technique. First, the titanium foils (99% purity) were polished with abrasive papers of grain sizes ranging from 320 to 2000, followed by ultrasonic cleaning in acetone, ethanol, and deionized water for 15 min and finally dried with pressurized nitrogen. The cleaned Ti foil (2.5 cm × 2.5 cm × 1 mm) was used as the anode, while Pt foil served as the counter electrode, both connected to a power supply at 60 V. These electrodes were immersed in an electrolyte bath containing ethylene glycol, 2% vol ultrapure water, and 1% vol ammonium fluoride with a 0.07M concentration for 40 min at a constant temperature of 25 °C. The anodized film was then sonicated in a 1 : 1 mixture of ethanol and distilled for 5 minutes to remove debris from the openings of the nanotubes. Afterward, the samples were rinsed with ethanol and distilled water. To crystallize the samples into the anatase phase, the prepared TiO_2-NTs were annealed at 400 °C for 3 hours (heating rate: 2 ° C min^{-1}).

The Pt/TiO_2-NTs samples was prepared using an electrodeposition method. The growth of Pt nanoparticles was carried out at room temperature in a three-electrode cell system; with TiO_2 nanotubes/Ti as the working electrode, a Pt foil as the counter electrode and all potentials recorded *versus* the saturated Ag/AgCl electrode. The electrolyte was an aqueous solution containing 0.5 mM H_2PtCl_6 and 0.5 mM H_2SO_4. The structure and particle size of the Pt nanoparticles were controlled by varying the deposition potential (0.1, 0.3, and 0.5 V). After electrodeposition, the electrode was removed from the solution and thoroughly washed with ultrapure water.

2.2. Target pollutants and reactor for VOC and bacteria removal

The photocatalytic efficiency of the prepared catalysts was evaluated using ethyl acetate (EA) as a VOC and *Escherichia coli* (*E. coli*) as a bacterial contaminant, targeting for the simultaneous degradation of both pollutants. Ethyl acetate, an organic liquid, is widely used in various applications, including paints, printing inks, plastics, and is commonly found in the agri-food industry. For bacterial testing, a diluted strain of *E. coli* (DSM 10198-0307-001), stored under refrigeration, was used. The degradation of gaseous and bacterial pollutants was studied in a batch reactor setup. The experiments were conducted with the pollutants individually (VOCs and bacteria separately) and in combination. Each test used 2 × 2 cm samples of the prepared catalysts placed in a 250 mL reactor, illuminated by a visible lamp (Sylvania Lynx-S 9W/840).

2.3. Photocatalytic degradation of ethyl acetate and bacterial inactivation

The photocatalytic degradation of ethyl acetate was investigated at different concentrations (5, 10, 15, and 20 mg m^{-3}) in batch experiments, all conducted under identical operating conditions. For each concentration, a catalyst was placed in a 250 mL batch reactor, which was sealed with a stopper and a septum to ensure airtight conditions (Fig. 1). A specific volume of ethyl acetate was introduced into the reactor according to the target concentration. Once prepared, the reactor was left to stabilize for 15 minutes to achieve equilibrium. Following this stabilization period, the visible lamp was activated to initiate the photocatalytic process. Samples were collected every 5 minutes to monitor the degradation of ethyl acetate over time using gas chromatography (GC) analysis.

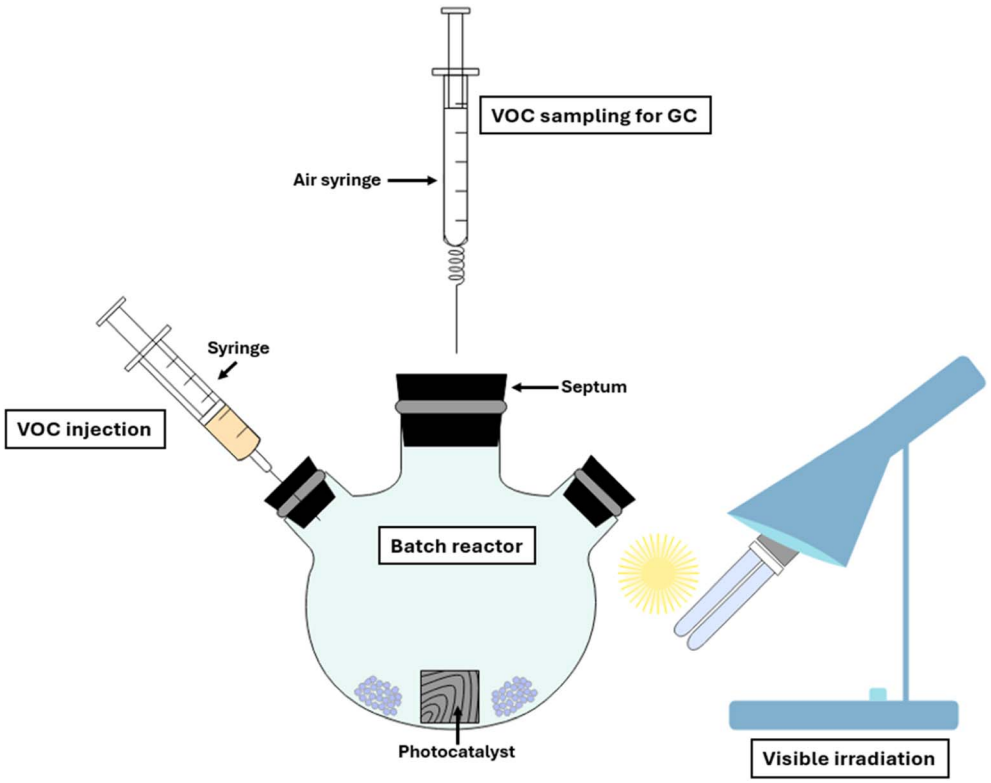

Fig. 1 Batch reactor configuration.

3. Results and discussion

3.1. Structural and morphological properties of catalysts

3.1.1. X-ray photoelectron spectroscopy (XPS) analysis. XPS is a valuable technique for detecting the surface composition of samples and was therefore performed to verify the deposition of Pt nanoparticles and determine the oxidation states of elements in the Pt/TiO_2-NTs system. Fig. 2 presents the XPS spectra of the Pt/TiO_2-NTs modified electrode. In Fig. 2a, the binding energies of Ti $2p_{3/2}$ and Ti $2p_{1/2}$ are around 458.7 and 464.1 eV respectively[20,21] suggesting a normal state of Ti^{4+} in TiO_2 indicating that the synthesis method did not influence the oxidation state of TiO_2. The O 1s XPS spectra in Fig. 2b can be deconvoluted into two peaks, corresponding to the lattice oxygen and surface hydroxyl species of TiO_2.[22,23] Fig. 2c shows the Pt 4f spectrum, which was analyzed and fitted with a doublet, with a separation of 3.4 eV so the two peaks located at 71.1 and 74.5 eV (Fig. 2c). The two peaks located at are assigned to Pt $4f_{7/2}$ and Pt $4f_{5/2}$ components of Pt^0 oxidation states, respectively[24,25] indicating the presence of metallic platinum on the surface. These results confirm that Pt was successfully deposited on the TiO_2-NTs substrate and that the electrodeposition method effectively reduced all Pt ions to metallic Pt, driven by the supply of excited electrons from the photo-excited TiO_2-NTs surface to adsorbed Pt ions.

3.1.2. Scanning electron microscopy (SEM) analysis. The SEM images in Fig. 3 depict the surface morphologies of annealed TiO_2 nanotubes grown on a Ti foil before and after the electrodeposition of Pt. Initially, all the samples exhibit highly ordered, smooth architecture with a regular nanoporous structure on the top surface, vertically aligned and tightly packed TiO_2 nanotubes are observed on the Ti substrate. These nanotubes exhibit an open top configuration, with an average diameter of approximately 80 nm and a wall thickness of about 10 nm. After electrodeposition, the Pt particles are randomly distributed on the TiO_2 nanotubes. The presence of elemental Pt, Ti and O is confirmed by the XPS results. In this study, A series of Pt/TiO_2-NTs catalysts prepared with various voltages (0.1 V, 0.3 V, and 0.5 V) were applied during the electrodeposition process to investig ate their influence on the deposition of Pt nanoparticles on TiO_2-NTs. The varying voltages significantly impacted the size, distribution, and overall morphology of the Pt nanoparticles.

At 0.1 V (image (b)), theTiO_2 nanotubes are clearly visible, displaying a regular nanostructure with a uniform nanoporous top layer decorated with Pt nanospheres. The Pt nanoparticles are small, with diameters ranging from 10 nm to 22 nm (average $\approx 16 \pm 3$ nm), and are homogeneously distributed on both the inner and outer walls of the TiO_2 nanotubes, as also observed in TEM images, without aggregation. This enhances the active surface area of the substrate.

At 0.3 V (image (c)), platinum nanoparticles exhibit a denser distribution, mostly located on the top of TiO_2 nanotubes, with diameters ranging from 40 nm to 110 nm (average $\approx 75 \pm 20$ nm). The nanoparticles are larger than those formed at 0.1 V, indicating more extensive nucleation and growth processes.

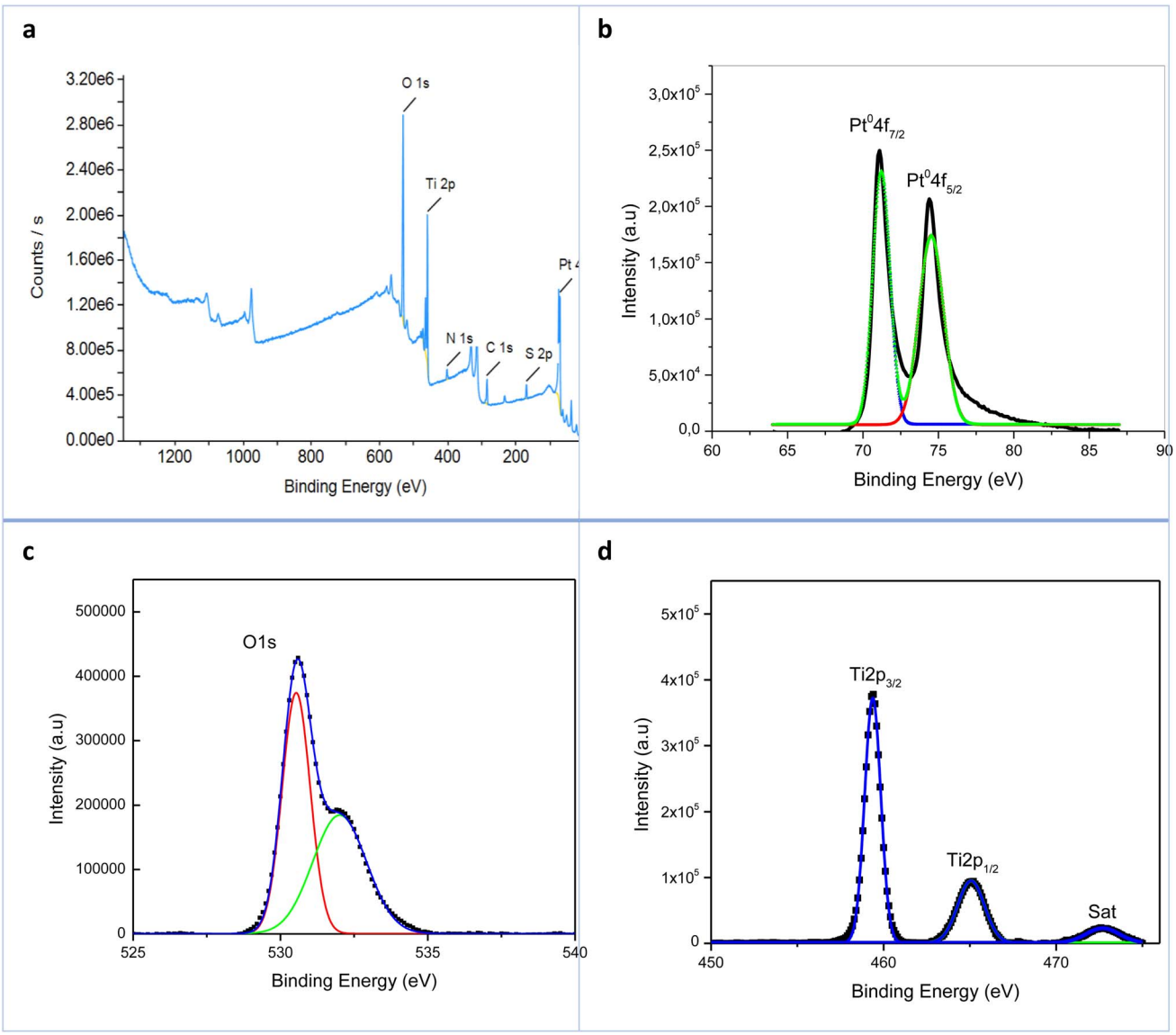

Fig. 2 XPS spectra of Pt-NPs/TiO_2-NTs prepared by electrodeposition under potential of about 0.1 V.

Aggregates of nanoparticles can be observed, suggesting initial growth.

At 0.5 V (image (d)), the surface of the nanotubes becomes progressively covered, especially on the top, by the platinum nanoparticles, which are significantly larger. Higher magnification reveals flower-like Pt particles with diameters ranging from 100 nm to 500 nm (average $\approx 300 \pm 80$ nm), consisting of multiple interlaced nanosheets, indicating significant growth in response to increased potential and favoring the formation of the Pt nanosheets. Under high electrodeposition current, a large number of Pt ions are reduced in a short period leading to agglomeration and decoration of Pt nanoparticles mainly on the outer of the tube wall.

These images highlight the progressive increase in nanoparticle size and density as the applied potential is raised, indicating the role of electrochemical conditions in controlling the morphology and distribution of platinum nanoparticles on TiO_2 nanotubes. This demonstrates that by electrodeposition process allows for precise control and tuning of Pt nanoparticles.

3.1.3. Transmission electron microscopy (TEM) analysis. To confirm the SEM results, TEM analysis was conducted. The TEM images provided further validation of the size, distribution, and morphology of the Pt nanoparticles deposited on the TiO_2-NTs at different voltages. TEM images of various Pt/TiO_2-NTs catalysts are presented in Fig. 4, showing that the electrodeposition method affects both the average size and distribution of Pt particle. The high-resolution of TEM image of Pt/TiO_2-NTs shows the presence of large number of TiO_2 nanotubes arranged randomly reveals the 1D nanostructure of TiO_2-NTs whose diameter is about 80 nm. These results confirm the formation of well-structured TiO_2-NTs and the presence of small dark spots, which are Pt nanoparticles of different sizes. For the sample deposited at 0.1 V Fig. 4b small Pt nanoparticles are uniformly distributed on the top layer and inner wall of TiO_2 nanotube; this homogeneous distribution without significant

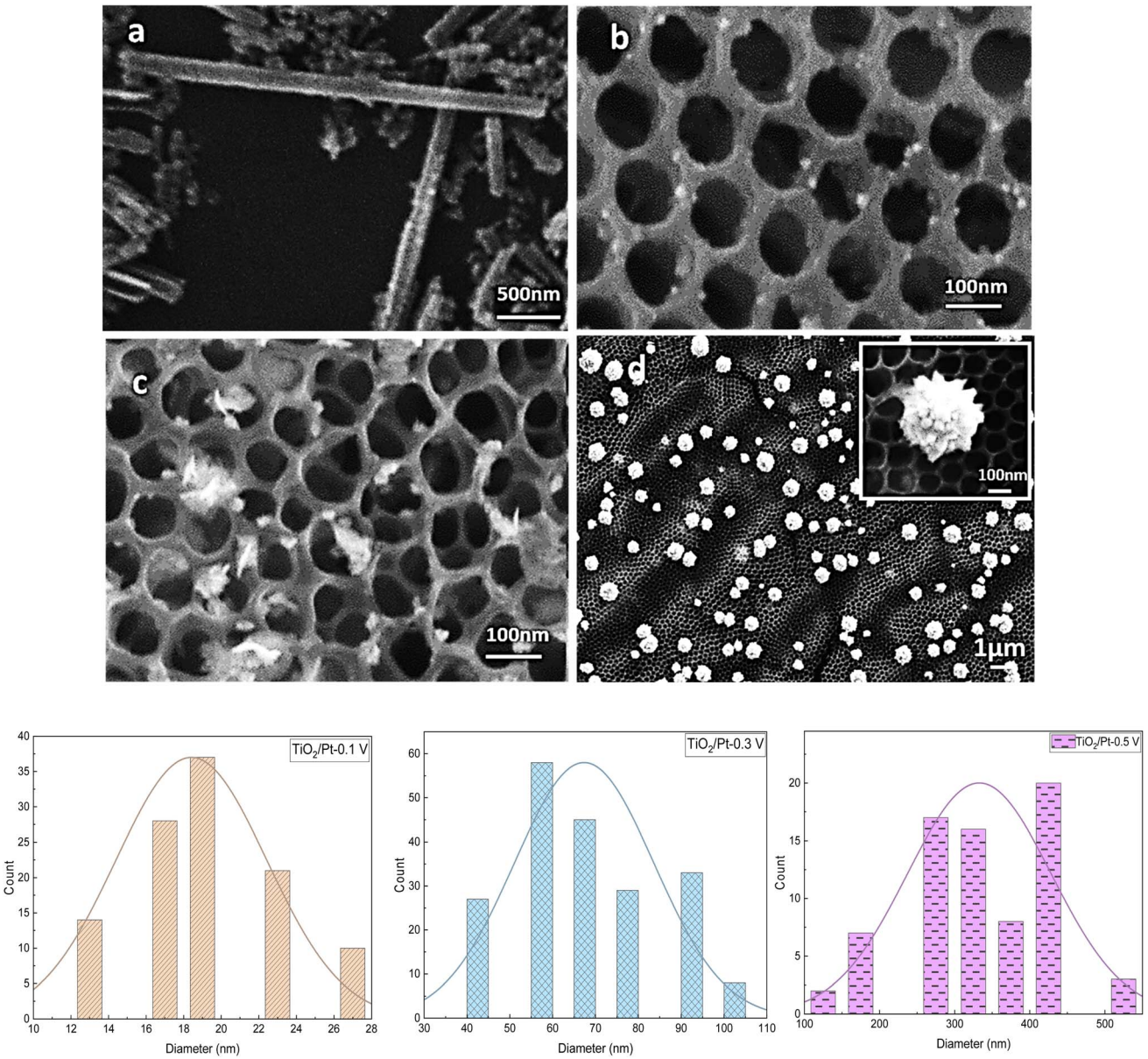

Fig. 3 The SEM images and nanoparticle size distribution of (a) TiO_2-NTs and Pt/TiO_2-NTs deposited in different voltages (b) 0.1 V, (c) 0.3 V and (d) 0.5 V.

aggregation indicates that the low voltage facilitated controlled deposition. At 0.5 V (Fig. 4d) large clusters of Pt with bigger sizes are clearly observed.

Thus, as the voltage increases from 0.1 V to 0.5 V, the size of Pt nanoparticles on TiO_2 nanotubes also increases, with higher voltages leading to faster deposition rates and larger, more aggregated nanoparticles. The electrodeposition method greatly influences the particle size and distribution of Pt nanoparticles which in turn affects the recombination of photogenerated charges.

3.2. Optical properties of catalysts

3.2.1. Photoluminescence (PL) analysis. The optical properties of the prepared samples were analyzed by PL and shown in Fig. 5; the PL emission spectra of modified TiO_2-NTs samples are compared with untreated TiO_2-NTs using an excitation wavelength of 265 nm. The broad peak around 400 nm was attributed to the free exciton emission is due to the electron transition from the conduction band to the valence band and the other peak around 497 nm originating from bound exciton emission occurs due to the presence of defects within the TiO_2 structure. According to Mercado *et al.*, the recombination of an electron from the valence band with a trapped hole is responsible for this emission.[26] A notable decrease in the PL intensity of Pt decorated TiO_2-NTs is evident. This intensity reduction is attributed to the presence of Pt nanoparticles on the TiO_2-NTs, which does not qualitatively change the form of the PL emission. With the introduction of Pt particles onto the surface of TiO_2 supports, a junction is formed between the TiO_2-NTs and

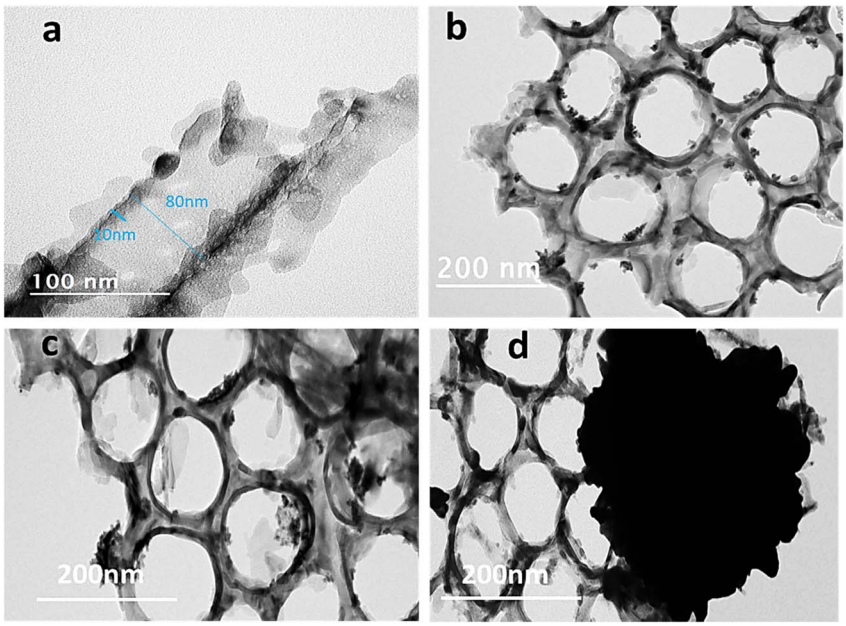

Fig. 4 TEM micrographs of the investigated Pt/TiO_2-NTs catalysts (a) prepared at different potential (b) 0.1 V, (c) 0.3 V and (d) 0.5 V.

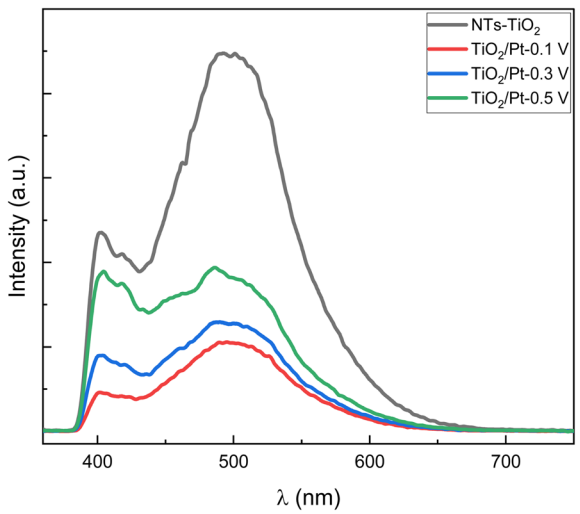

Fig. 5 Photoluminescence spectra of TiO_2-NTs decorated with Pt-NPs prepared under applying different potential.

Pt nanoparticles, enabling the transport of electrons from TiO_2-NTs to Pt nanoparticles.

Pt-nanoparticles act as electron traps, suppressing charge carrier combination and consequently decreasing PL intensity.[27] Notably, Pt/TiO_2-NTs sample prepared at 0.1 V exhibits the lowest PL intensity, which is characterized by homogeneously dispersed, small Pt nanoparticles.[28] In contract, the Pt/TiO_2-NTs sample prepared at 0.5 V, where Pt clusters are observed, shows higher PL intensity likely due to the large size of Pt aggregates, which may limit the electron transport and enhance the electron–hole recombination. These results demonstrate that particles size significant impacts the efficiency of Pt nanoparticles in charge separation process.

3.2.2. Photoluminescence (PL) analysis. UV-visible diffuse reflectance spectroscopy (DRS) analysis (Fig. 6) reveals a significant enhancement in optical absorption upon Pt decoration of TiO_2. While pure TiO_2 shows strong absorption in the UV region, Pt-decorated samples exhibit extended absorption into the visible range. This red-shift is mainly attributed to the localized surface plasmon resonance (LSPR) of Pt nanoparticles and the formation of metal–semiconductor junctions that facilitate charge separation.[29] The sample prepared at 0.5 V shows the highest overall absorbance, indicating higher Pt loading. However, despite this enhanced light absorption, it exhibits lower photocatalytic activity compared to the sample

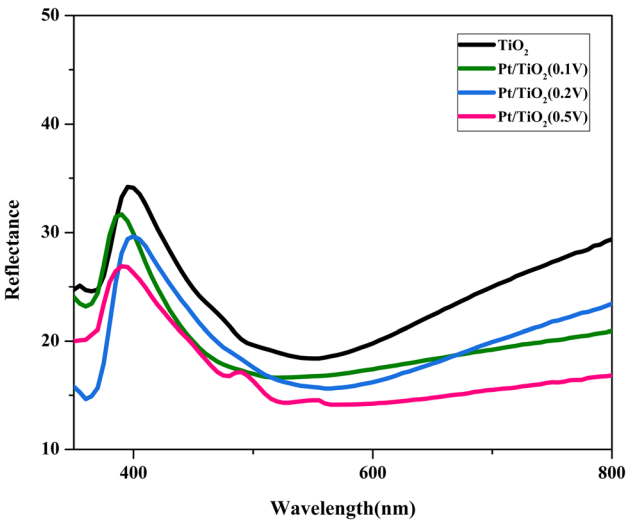

Fig. 6 UV-visible diffuse reflectance spectra of TiO_2-NTs decorated with Pt-NPs.

prepared at 0.1 V. This can be explained by the fact that larger and more aggregated Pt nanoparticles, likely formed at higher deposition potentials, can act as recombination centers, partially block light penetration, shield the TiO_2 surface from incident light and cover active TiO_2 sites. As a result, a portion of the light is absorbed by Pt instead of reaching the TiO_2, reducing the generation of photogenerated charge carriers.[30] Therefore, optimal nanoparticle size, dispersion and homogeneous distribution are more crucial than absorbance alone in achieving efficient photocatalysis.

4. Photocatalytic application

4.1. The effect of Pt-NPs size on VOC degradation

To evaluate the influence of platinum deposition voltage on the photocatalytic degradation efficiency of volatile organic compounds (VOCs), ethyl acetate was selected as the model pollutant. An initial volume of 5 μL of ethyl acetate was accurately injected into a batch reactor, establishing a concentration of 5 mg m^{-3} within the reactor.

The degradation process was then monitored under visible light irradiation, utilizing various catalysts synthesized at different platinum deposition voltages to assess their photocatalytic performance (Fig. 7). The degradation results over time are illustrated in Fig. 6. It is evident that photocatalytic efficiency varies with Pt nanoparticles size, which is determined by the applied voltage during platinum deposition on TiO_2.[31] Among the catalysts tested, the TiO_2/Pt-0.1 V catalyst exhibited the highest photocatalytic activity, achieving total degradation within 150 minutes of visible light exposure. This superior performance at 0.1 V can be attributed to several factors. TEM and SEM images confirm that the lower deposition voltage of 0.1 V produces smaller platinum nanoparticles, which are more uniformly distributed on the walls of the TiO_2 nanotubes. The smaller and well-dispersed nanoparticles increase the available active surface area for photocatalytic reactions, thus improving the overall efficiency of the process. Additionally, platinum acts as a co-catalyst facilitates the separation of electron–hole pairs generated under visible light irradiation, thereby reducing their recombination and increasing the lifetime of charge carriers. This allows for more efficient oxidation of ethyl acetate molecules. Previous studies[32,33] have also shown that the size and dispersion of platinum nanoparticles have a direct impact on photocatalytic efficiency.

In conclusion, platinum deposition significantly enhances the photocatalytic degradation of ethyl acetate, and optimal activity is achieved at a lower deposition voltage of 0.1 V, resulting in smaller, well-dispersed platinum nanoparticles with higher surface area and more effective charge separation, a low charge carrier recombination rate is associated with high photocatalytic activity. For similar findings, numerous studies have investigated the effect of platinum nanoparticle size on TiO_2 photocatalysts, consistently demonstrating that smaller Pt nanoparticles yield the highest photocatalytic efficiency. In our previous article, we examined platinum deposition using two distinct methods, showing that smaller Pt nanoparticles significantly improved the efficiency of VOC and bacterial removal, attributed to their larger surface area and reduced electron–hole recombination rates, highlighting the critical role of nanoparticle size in enhancing photocatalytic performance.[31]

4.2. The effect of ethyl acetate (EA) concentration and kinetic constants

The variation in platinum deposition voltage results in different nanoparticle sizes, influencing photocatalytic activity, with the TiO_2/Pt-0.1 V catalyst demonstrating the highest performance. Building on this, we investigated the effect of varying ethyl acetate (EA) concentrations on photocatalytic degradation kinetics using this optimal catalyst. Fig. 8 presents the degradation of EA at different initial concentrations with the TiO_2/Pt-

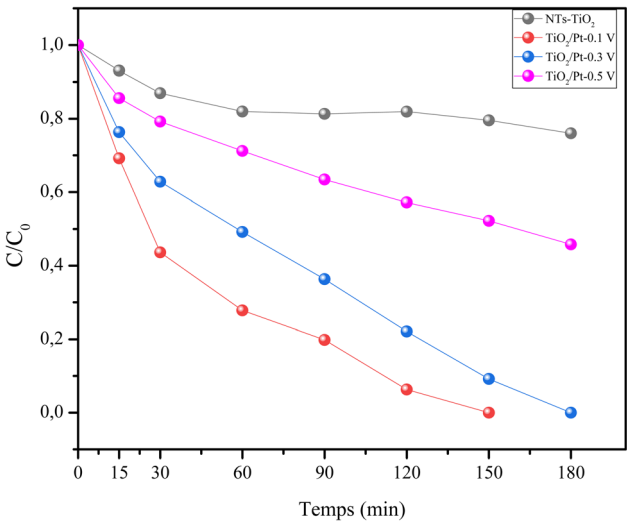

Fig. 7 Photocatalytic degradation of ethyl acetate as a function of time of pure and Pt-NPs decorated TiO_2-NTs prepared by electrodeposition at different potentials.

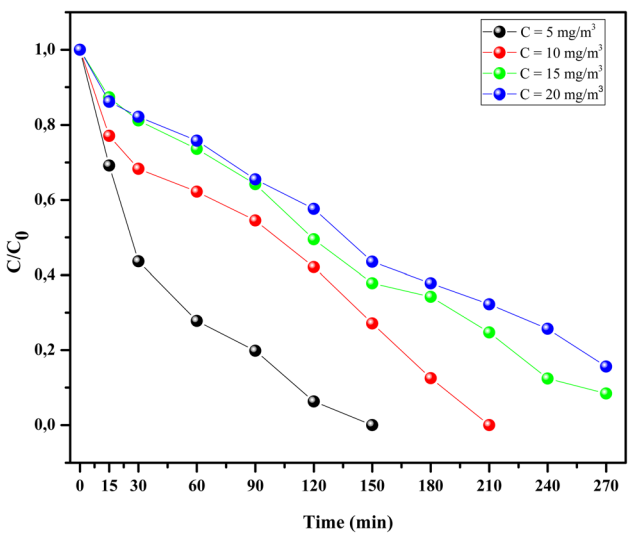

Fig. 8 Ethyl acetate degradation as a function of time for different initial concentrations using Pt/TiO_2 catalyst prepared at 0.1 V.

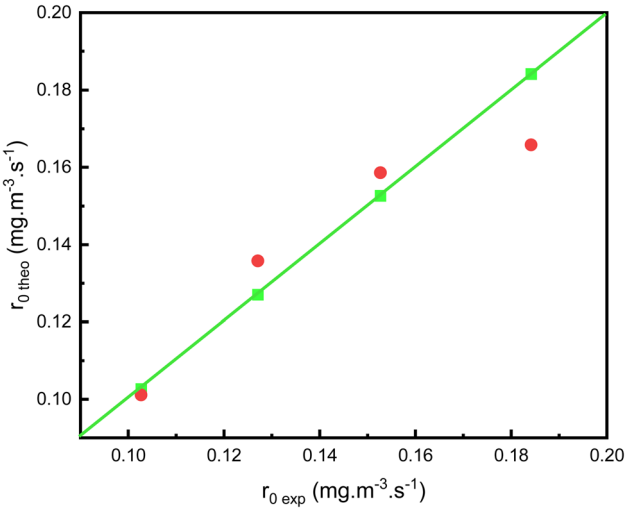

Fig. 9 Representation of the experimental degradation rate as a function of the theoretical degradation rate.

0.1 V catalyst. Total degradation was achieved for the two lowest pollutant concentrations. These results indicate that increasing the EA concentration diminishes photocatalytic activity.

This inhibition in pollutant removal can be attributed to the increased number of pollutant molecules in the reactor while the catalyst generates a constant number of reactive oxygen species (ROS) such OH° and O_2^-., which are responsible for pollutant degradation.[34] Consequently, the competition between EA molecules for the generated ROS explains the decrease in photocatalytic activity. As the pollutant concentration increases, the catalyst becomes saturated, and its efficiency is inhibited. Additionally, this study allows us to determine the different degradation rate constants.

We used Langmuir–Hinshelwood (L–H) model to describe the removal efficiency of TiO_2/Pt-0.1 V catalyst and determine the degradation constants:[18]:

$$r_0 = \frac{d[VOC]}{dt} = k_c \times \frac{K[VOC]_0}{1 + K[VOC]_0}$$

where r_0 the initial rate of photocatalytic degradation (mg m^{-3} min^{-1}), k_c the kinetic constant (mg m^{-3} min^{-1}), K the adsorption constant (m^3 mg^{-1}) and [VOC] is the initial concentration of ethyl acetate (mg m^{-3}). These constants could be obtained by plotting $1/r_0 = f(1/[VOC])$ and the linearized equation is:

$$\frac{1}{r_0} = \frac{1}{K \times k_c} \times \frac{1}{[VOC]} + \frac{1}{k_c}$$

The analysis of the empirical degradation rate as a function of the experimental rate reveals a significant correlation (Fig. 9). The kinetic and adsorption constants were obtained and presented in Table 1.

We obtain a kinetic constant $k_c = 0.04$ mg m^{-3} min^{-1} and $K = 5.5$ m^3 mg^{-1}. These results show that our catalyst TiO_2/Pt-0.1 V exhibits a high rate of VOC degradation compared to other catalysts. Khezami *et al.* obtained a kinetic constant $k_c = 0.064$ mg m^{-3} min^{-1} using TiO_2/Pt catalyst for the degradation of Cyclohexane.[35] We conclude that platinum nanoparticles enhance VOCs degradation compared to TiO_2 alone and platinum demonstrates superior degradation performance compared to other noble metals.[33,36]

4.3. Simultaneous removal and degradation mechanism

After dealing with VOC (EA) degradation, our catalysts were tested for bacterial inactivation (*E. coli*). For this simultaneous removal study, a concentration ~3.5×10^4 (CFU mL^{-1}) of the bacterial strain was applied onto the catalyst, and a concentration of 5 mg m^{-3} of EA is injected into the reactor. The degradation of pollutant over time under visible irradiation is presented in Fig. 10. Regarding bacteria inactivation, we note that the presence of the VOC does not affect the inactivation of bacteria which reaches total degradation in less than 90 minutes using the efficient catalyst. Pure TiO_2 nanotubes show significant activity for bacteria removal, achieving total degradation after 150 minutes of irradiation. The bacteria removal by photocatalysis used TiO_2 with noble metals was investigated in previous studies and pure titanium dioxide nanotubes showed and important removal rate especially under UV light.[37,38] However, noble metals nanoparticles were mentioned for the elimination of several bacteria and the enhancement of the photocatalytic activity of catalyst. Based on previous results for *E. coli* inactivation our catalyst TiO_2/Pt-0.1 V achieved superior activity compared to other results, reaching total degradation in a shorter irradiation time.[37,39,40] For ethyl acetate degradation, we remark that the addition of bacteria inside the reactor reduces EA degradation. Such behavior could be explained by the competition between pollutants for degradation by generated reactive species and the presence of different pollutants or the increasing of pollutants molecules reduce the removal efficiency.[34]

This study revealed the photocatalytic activity of TiO_2 nanotubes for VOC and bacteria degradation. It also demonstrated the significance enhancement provided by the addition of platinum nanoparticles. To understand how we obtained such an improvement in the elimination rate of pollutants we must first identify the agent responsible for the pollutants degradation and what happens during semiconductor–metal contact which enhance the photodegradation. The reactive oxygen species (ROS) generated during the excitation of our TiO_2 semiconductor are the agents responsible for the

Table 1 Adsorption and kinetic constants for TiO_2/Pt-0.1 V

Catalyst	k_c: kinetic constant of L–H (mg m^{-3} min^{-1})	K: adsorption constant of L–H (m^3 mg^{-1})
Pt/TiO_2-NTs	0.04	5.5

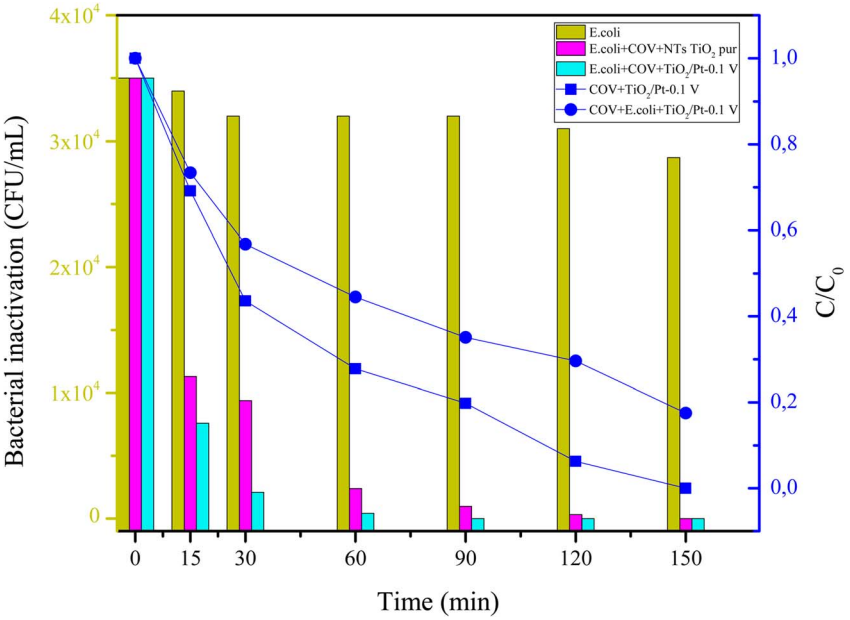

Fig. 10 Simultaneous removal of *E. coli* and ethyl acetate as a function of irradiation time for pure TiO_2 nanotubes and Pt/TiO_2-NTs.

degradation of pollutants. Belkessa *et al.* demonstrated the reactive species relevant to VOC removal using TiO_2 as a photocatalyst. Using superoxide dismutase and tert-butanol as scavengers, the contribution of superoxide radical anion ($O_2^{\bullet -}$) and hydroxyl radicals ($OH^{\bullet}$) was reported for the degradation of ethylbenzene.[41] Indeed, these generated species ($OH^{\bullet}$, $O_2^{\bullet -}$) are strongly oxidized; they have the ability to decompose organic pollutants and inactivate bacteria by the destruction of its membrane.[42,43] However, the generation of these reactive species within the semiconductor is limited by several factors such as the strong recombination of TiO_2 pair electron–holes responsible for ROS production. This is where the role of adding platinum nanoparticles becomes crucial; platinum deposition onto TiO_2 nanotubes can limit the recombination of electron–hole pairs. During semiconductor–metal (TiO_2–Pt) contact, we will get a passage of electrons from the conduction band of semiconductor to platinum nanoparticles, which creates a space charge zone at the contact surface. This Schottky junction inhibits the recombination of electron–hole pairs by trapping electrons in the metal nanoparticles.[25,44] These trapped electrons could participate in ROS production which enhance the photodegradation of several pollutants. Reactive species are capable to break down all molecule's bonds of ethyl acetate until mineralization.[45] The same for bacteria, generated ROS destroy *E. coli* by the disruption of membrane cell and the destruction of DNA which inactivate the bacteria.[46] So, we revealed the species responsible for the degradation of EA and *E. coli* as well as the mechanism and effect of adding platinum nanoparticles (Fig. 11).

We can explain the mechanism as follows: under light irradiation, TiO_2 generates electron–hole pairs (e^-/h^+). The presence of Pt nanoparticles serves as effective electron acceptors, promoting rapid electron transfer from the conduction band of

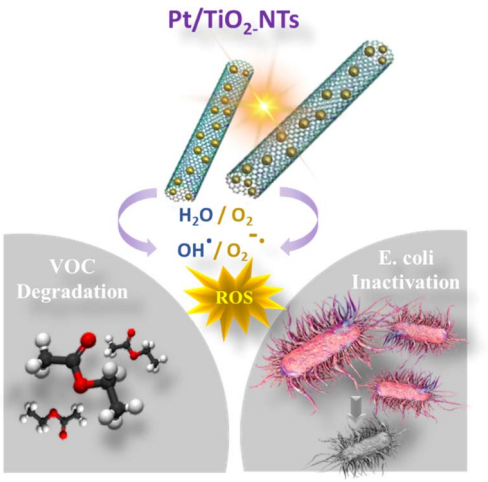

Fig. 11 EA and *E. coli* plausible degradation mechanism.

TiO_2 to the Pt sites. This process minimizes electron–hole recombination and increases the availability of holes for oxidative reactions. The trapped electrons on the Pt nanoparticles can reduce molecular oxygen (O_2) to generate reactive oxygen species. These ROS are highly reactive and can effectively degrade volatile organic compounds (VOCs) and bacterial cells in indoor air, resulting in enhanced indoor air quality.

5. Conclusions

In this study, we successfully deposited platinum (Pt) nanoparticles onto titanium dioxide nanotubes (TiO_2-NTs) using a voltage-controlled electrodeposition approach, achieving a novel level of control over nanoparticle size. The applied deposition voltage played a crucial role in determining Pt

particle size and distribution, with smaller particles (10–22 nm) obtained at 0.1 V showing superior photocatalytic performance. The TiO_2/Pt-0.1 V catalyst exhibited remarkable activity, achieving complete degradation of ethyl acetate (EA) within 150 minutes under visible light irradiation. This catalyst also demonstrated significant antibacterial properties against *E. coli*. The results highlight the critical role of nanoparticle size optimization in enhancing photocatalytic activity. Our findings highlight the effectiveness of voltage-controlled deposition in tailoring catalyst properties for enhancing indoor air quality.

Data availability

The authors confirm that the data supporting the findings of this study are available within the article.

Conflicts of interest

The authors declare that they have no conflict of interest.

Funding statement

This work was supported and funded by the Deanship of Scientific Research at Imam Mohammad Ibn Saud Islamic University (IMSIU) (grant number IMSIU-DDRSP2502).

References

1 Y. Zhu, H. Shen, Q. Ai, Y. Feng, B. Shin, M. Gonzales, Y. Yan, Z. He, X. Huang, X. Zhang, Y. Han, P. M. Ajayan, Q. Li and J. Lou, *Nano Lett.*, 2024, **24**, 13718–13726.
2 S. Elbasuney, A. M. El-Khawaga, M. A. Elsayed, A. Elsaidy and M. A. Correa-Duarte, *Sci. Rep.*, 2023, **13**, 13819.
3 E. Nardell and R. Nathavitharana, *Lancet*, 2019, **394**, 1009–1010.
4 R. Li, Y. Huang, D. Zhu, W. Ho, J. Cao and S. Lee, *Environ. Sci. Technol.*, 2021, **55**, 4054–4063.
5 Y. Huang, P. Wang, Z. Wang, Y. Rao, J. Cao, S. Pu, W. Ho and S. C. Lee, *Appl. Catal. B Environ.*, 2019, **240**, 122–131.
6 P.-A. Bourgeois, E. Puzenat, L. Peruchon, F. Simonet, D. Chevalier, E. Deflin, C. Brochier and C. Guillard, *Appl. Catal. B Environ.*, 2012, **128**, 171–178.
7 J. Zhao and X. Yang, *Build. Environ.*, 2003, **38**, 645–654.
8 P. V. Laxma Reddy, B. Kavitha, P. A. Kumar Reddy and K.-H. Kim, *Environ. Res.*, 2017, **154**, 296–303.
9 Z. Shayegan, C.-S. Lee and F. Haghighat, *Chem. Eng. J.*, 2018, **334**, 2408–2439.
10 N. Belkessa, A. A. Assadi, P. N. Tri and A. Bouzaza, *Catal. Today*, 2025, **458**, 115380.
11 C. H. A. Tsang, K. Li, Y. Zeng, W. Zhao, T. Zhang, Y. Zhan, R. Xie, D. Y. C. Leung and H. Huang, *Environ. Int.*, 2019, **125**, 200–228.
12 O. K. Varghese, D. Gong, M. Paulose, K. G. Ong, E. C. Dickey and C. A. Grimes, *Adv. Mater.*, 2003, **15**, 624–627.
13 A. A. Assadi, A. Bouzaza, M. Lemasle and D. Wolbert, *Chem. Eng. Res. Des.*, 2015, **93**, 640–651.
14 S. A. Ansari, F. Khan and A. Ahmad, *Int. J. Anal. Chem.*, 2016, **2016**, 1–10.
15 X. Zhu, C. Jin, X.-S. Li, J.-L. Liu, Z.-G. Sun, C. Shi, X. Li and A.-M. Zhu, *ACS Catal.*, 2017, **7**, 6514–6524.
16 A. Zielińska-Jurek, *J. Nanomater.*, 2014, **2014**, 1–17.
17 A. L. Linsebigler, G. Lu and J. T. Yates, *Chem. Rev.*, 1995, **95**, 735–758.
18 A. Kane, L. Chafiq, S. Dalhatou, P. Bonnet, M. Nasr, N. Gaillard, J. M. D. Dikdim, G. Monier, A. A. Assadi and H. Zeghioud, *J. Photochem. Photobiol., A*, 2022, **430**, 113971.
19 A. Zielińska, E. Kowalska, J. W. Sobczak, I. Łącka, M. Gazda, B. Ohtani, J. Hupka and A. Zaleska, *Sep. Purif. Technol.*, 2010, **72**, 309–318.
20 Z. H. N. Al Azri, V. Jovic, W. T. Chen, D. S. Waterhouse, J. B. Metson and G. I. N. Waterhouse, *Int. J. Nanotechnol.*, 2014, **11**, 695.
21 C. Wu, S. Xue, Z. Qin, M. Nazari, G. Yang, S. Yue, T. Tong, H. Ghasemi, F. C. R. Hernandez, S. Xue, D. Zhang, H. Wang, Z. M. Wang, S. Pu and J. Bao, *Appl. Catal. B Environ.*, 2021, **282**, 119557.
22 B. Xin, P. Wang, D. Ding, J. Liu, Z. Ren and H. Fu, *Appl. Surf. Sci.*, 2008, **254**, 2569–2574.
23 S. K. Poznyak, V. I. Pergushov, A. I. Kokorin, A. I. Kulak and C. W. Schläpfer, *J. Phys. Chem. B*, 1999, **103**, 1308–1315.
24 C. Wu, L. Fang, F. Ding, G. Mao, X. Huang and S. Lu, *Chem. Phys. Lett.*, 2023, **826**, 140650.
25 N. Lakshmanareddy, V. Navakoteswara Rao, K. K. Cheralathan, E. P. Subramaniam and M. V. Shankar, *J. Colloid Interface Sci.*, 2019, **538**, 83–98.
26 J. L. McHale and C. C. Mercado, *MRS Proc.*, 2010, **1268**, 310.
27 F. Wu, X. Hu, J. Fan, E. Liu, T. Sun, L. Kang, W. Hou, C. Zhu and H. Liu, *Plasmonics*, 2013, **8**, 501–508.
28 E. Liu, L. Kang, Y. Yang, T. Sun, X. Hu, C. Zhu, H. Liu, Q. Wang, X. Li and J. Fan, *Nanotechnology*, 2014, **25**, 165401.
29 A. FUJISHIMA and K. HONDA, *Nature*, 1972, **238**, 37–38.
30 J. Zhang, L. Li and G. Li, *Int. J. Photoenergy*, 2012, **2012**, 1–7.
31 M. A. Hajjaji, K. Missaoui, K. Trabelsi, A. Bouzaza, A. Hajjaji, B. Bessais and A. A. Assadi, *J. Photochem. Photobiol. A Chem.*, 2025, **458**, 115975.
32 D. Wang, Z.-P. Liu and W.-M. Yang, *ACS Catal.*, 2018, **8**, 7270–7278.
33 E. Grabowska, M. Marchelek, T. Klimczuk, G. Trykowski and A. Zaleska-Medynska, *J. Mol. Catal. A Chem.*, 2016, **423**, 191–206.
34 W. Abou Saoud, A. A. Assadi, M. Guiza, A. Bouzaza, W. Aboussaoud, I. Soutrel, A. Ouederni, D. Wolbert and S. Rtimi, *Chem. Eng. J.*, 2018, **344**, 165–172.
35 L. Khezami, I. Lounissi, A. Hajjaji, A. Guesmi, A. A. Assadi and B. Bessais, *Materials (Basel).*, 2021, **14**, 7341.
36 G. Xu, H. Liu, J. Wang, J. Lv, Z. Zheng and Y. Wu, *Electrochim. Acta*, 2014, **121**, 194–202.
37 K.-S. Moon, E.-J. Choi, J.-M. Bae, Y.-B. Park and S. Oh, *Materials (Basel)*, 2020, **13**, 3721.
38 S. Pigeot-Rémy, F. Simonet, E. Errazuriz-Cerda, J. C. Lazzaroni, D. Atlan and C. Guillard, *Appl. Catal. B Environ.*, 2011, **104**, 390–398.

39 S. Karoui, A. A. Assadi, A. Meslem and B. Abdelkrim, *Food Biosci.*, 2024, **61**, 104771.
40 A. A. Assadi, *Materials*, 2024, **17**, 296.
41 N. Belkessa, Y. Serhane, A. Bouzaza, L. Khezami and A. A. Assadi, *Environ. Sci. Pollut. Res.*, 2022, **30**, 35745–35756.
42 A. Esrafili, M. Salimi, A. jonidi jafari, H. Reza Sobhi, M. Gholami and R. Rezaei Kalantary, *J. Mol. Liq.*, 2022, **352**, 118685.
43 S. Karoui, A. A. Assadi, A. Ghorbal, L. Khezami, A. Assadi, S. Loganathan and A. Amrane, *J. Water Process Eng.*, 2023, **56**, 104448.
44 C. Vanlalhmingmawia, S. M. Lee and D. Tiwari, *J. Water Process Eng.*, 2023, **51**, 103360.
45 H. Wang, S. Chen, Z. Wang, Y. Zhou and Z. Wu, *Appl. Catal. B Environ.*, 2019, **254**, 339–350.
46 T. O. Ajiboye, S. O. Babalola and D. C. Onwudiwe, *Appl. Sci.*, 2021, **11**, 1313.